



Modeling the dynamics of an elastic rod with intrinsic curvature and twist using a regularized Stokes formulation



Sarah D. Olson^{a,*}, Sookkyung Lim^b, Ricardo Cortez^c

^a Department of Mathematical Sciences, Worcester Polytechnic Institute, 100 Institute Road, Worcester, MA 01609, USA

^b Department of Mathematical Sciences, University of Cincinnati, 4199 French Hall West, Cincinnati, OH 45221, USA

^c Mathematics Department, Tulane University, 6823 St. Charles Ave., New Orleans, LA 70118, USA

ARTICLE INFO

Article history:

Received 20 March 2012

Received in revised form 12 December 2012

Accepted 20 December 2012

Available online 3 January 2013

Keywords:

Regularized Stokeslets

Fluid–structure interaction

Kirchhoff rod theory

Immersed boundary method

ABSTRACT

We develop a Lagrangian numerical algorithm for an elastic rod immersed in a viscous, incompressible fluid at zero Reynolds number. The elasticity of the rod is described by a version of the Kirchhoff rod model, where intrinsic curvature and twist are prescribed, and the fluid is governed by the Stokes equations in \mathbb{R}^3 . The elastic rod is represented by a space curve corresponding to the centerline of the rod and an orthonormal triad, which encodes the bend and twist of the rod. In this method, the differences between the rod configuration and its intrinsic shape generate force and torque along the centerline. The coupling to the fluid is accomplished by the use of the method of regularized Stokeslets for the force and regularized rotlets for the torque. This technique smooths out the singularity in the fundamental solutions of the Stokes equations for the computation of the velocity of the rod centerline. In addition, the computation of the angular velocity of the rod requires the use of regularized (potential) dipoles. As a benchmark problem, we consider open and closed rods with intrinsic curvature and twist in a viscous fluid. Equilibrium configurations and dynamic instabilities are compared with known results in elastic rod theory. For cases when the exact solution is unknown, the numerical results are compared to those produced by the generalized immersed boundary (gIB) method, where the fluid is governed by the Navier–Stokes equations with small Reynolds number on a finite (periodic) domain. It is shown that the regularization method combined with Kirchhoff rod theory contributes substantially to the reduction of computation time and efficient memory usage in comparison to the gIB method. We also illustrate how the regularized method can be used to model microorganism motility where the organism is propelled by a flagellum propagating sinusoidal waves. The swimming speeds of this flagellum using the regularized Stokes formulation are matched well with classical asymptotic results of Taylor's infinite cylinder in terms of frequency and amplitude of the undulation.

© 2013 Elsevier Inc. All rights reserved.

1. Introduction

The classical Kirchhoff rod theory [1] has been employed to study the dynamical instabilities of elastic rods [2–6] and applied to various problems in which long, thin rodlike structures at macro and micro scales are involved. Most of the work focuses on the rod dynamic instabilities or steady configurations in the absence of any environment [7–12,3]. Initial models that include the effect of a fluid medium around the rod used some type of artificial damping [13,5] to account for the drag

* Corresponding author. Tel.: +1 508 831 4940.

E-mail addresses: sdolson@wpi.edu (S.D. Olson), sookkyung.lim@uc.edu (S. Lim), rcortez@tulane.edu (R. Cortez).

within the fluid or used resistive force theory for the case of a Stokes fluid [14]. More recently, Lim et al. have developed a more comprehensive model where the rod is immersed in a fluid by coupling the rod dynamics with the Navier–Stokes equations [15–17].

The importance of including the fluid medium in the rod dynamics is evident in the many applications of elastic rod models, such as the study of supercoiling dynamics of DNA [18–20], bacterial flagellar behavior [21], and growth of bacteria [22–24]. In many physical and biological applications, we are interested in modeling an elastic filament or thin rodlike structure that is immersed in a fluid, where the outcome of interest may be the flow around the object, interactions of structures, or possibly the swimming speed if the structure is actively bending. Since most of these applications are focused on small length scale filamentous structures within the fluid, where viscous forces dominate, it is natural to model the dynamics of elastic rods in a viscous fluid governed by a Kirchhoff rod formulation and the Stokes equations.

The goal of this work is to present a grid free numerical algorithm for thin rodlike structures in the limit of zero Reynolds number that captures the bend and twist of an elastic rod. The elastic rod is described by a three-dimensional space curve representing the centerline of the rod and an associated orthonormal triad along the rod, encoding the amount of bend and twist along the rod. The differences between the rod configuration at a given time and its intrinsic shape generate forces and torques along the centerline. These act on the fluid, generating flows that affect the rod itself. This coupling can be modeled by a variety of methods. In the Stokes regime, it is known that boundary integral methods [25–27], slender body theory [28–30], the immersed boundary (IB) method [31], and the method of regularized Stokeslets [32,33] have been used to model slender bodies immersed in a fluid. Biological applications using the method of regularized Stokeslets include modeling arthropod filiform hairs [34], flagellar bundling of bacteria [35], spirochete motility [33], sperm swimming near surfaces [36], and hyperactivated sperm motility [37]; however, the formulation has never been coupled with the elastic rod dynamics. Slender body theory has also been extended to study growing elastic filaments [30] and the interaction of flexible filaments [38]. In all of these examples, each structure was described by a centerline (or centerlines), which captured the shearing and extension/compression, but the twist was neglected.

In the past few years the generalized immersed boundary (gIB) method has been developed and improved to study the dynamics of filamentous structures such as marine cables and bacterial flagella [15–17,39]. In this method, the dynamics of the rod are governed by a Kirchhoff rod model, where the bend and twist of the rod are captured. The fundamental mathematical framework is the same as the original IB method; however, in the gIB method the immersed boundary applies torques as well as forces to the surrounding fluid, and the immersed boundary rotates at the local angular velocity of the fluid as well as translates at the local fluid velocity. A possible disadvantage, but not always, of the IB method is that since the fluid is governed by the full Navier–Stokes equations, the computation time is expensive, especially, in three-dimensional settings. One way to overcome this disadvantage is to use an adaptive version of the numerical method [15], and another way is to use fundamental solutions for problems at zero Reynolds number, which will be presented here.

We will focus on a regularized Stokes formulation in which the immersed structure takes the form of Kirchhoff's elastic rod. In this formulation, we are able to exploit the linearity of the Stokes equations to represent the local linear and angular velocity as a superposition of regularized fundamental solutions. Since this is strictly a Lagrangian method, we only evaluate the linear and angular fluid velocity at the centerline of the rod, making the method computationally efficient. To investigate the utility of the regularized Stokes framework, we illustrate how this method can be used to model waves of bending in a flagellum. We also conduct validation studies and compare the results with known solutions from elastic rod theory. In cases when solutions are unknown, the numerical results are compared to those produced by the gIB method, where the fluid is described by the Navier–Stokes equations with small Reynolds number.

2. Kirchhoff rod model

Variations of Kirchhoff models for elastic rods have been developed and applied to various modeling problems [8,10,1,3–5,40]. In this work we adopt a version of the Kirchhoff rod model, as developed by Lim et al. [16,17], to study the dynamics of an elastic rod interacting with an incompressible, viscous fluid. As in the standard Kirchhoff rod model, the rod can be represented by a space curve $\mathbf{X}(s)$ and an associated orthonormal triad $\{\mathbf{D}^1(s), \mathbf{D}^2(s), \mathbf{D}^3(s)\}$ for $0 \leq s \leq L$, where L is the length of the unstressed rod and s is a Lagrangian parameter that is initialized as arclength. It is assumed that the rod is homogeneous and isotropic. In contrast to the standard Kirchhoff rod theory, we do not exactly enforce the constraint that \mathbf{D}^3 is to be aligned with the tangent vector to the rod

$$\partial \mathbf{X} / \partial s = \mathbf{D}^3. \quad (1)$$

Similarly, we do not enforce an inextensibility constraint for the rod,

$$\|\partial \mathbf{X} / \partial s\| = 1, \quad (2)$$

where $\|\cdot\|$ denotes the Euclidean norm. Instead, we use a postulated energy penalty associated with the rod that tends to maintain these two conditions approximately (see Eq. (6) below).

We consider an elastic rod in its relaxed form such that \mathbf{D}^1 and \mathbf{D}^2 are perpendicular to the axis of the rod and aligned with the principal axes of the cross section, capturing the bend and twist of the rod. The director basis also forms a right-handed triad, $\mathbf{D}^i \cdot \mathbf{D}^j = \delta_{ij}$, where δ_{ij} is the Kronecker delta. Internal forces and couples are transmitted across a section of

the rod at s and are denoted by $\mathbf{F}(s)$ and $\mathbf{N}(s)$, respectively. As derived in [16], averaging the stresses on an arbitrary cross section, the force and torque balance give:

$$0 = \mathbf{f} + \frac{\partial \mathbf{F}}{\partial s}, \tag{3a}$$

$$0 = \mathbf{n} + \frac{\partial \mathbf{N}}{\partial s} + \left(\frac{\partial \mathbf{X}}{\partial s} \times \mathbf{F} \right), \tag{3b}$$

where the force density \mathbf{f} and torque density \mathbf{n} (with respect to the measure ds) exerted by the fluid on the rod are expanded in terms of the orthonormal triad $\{\mathbf{D}^1, \mathbf{D}^2, \mathbf{D}^3\}$. Similarly, the internal force \mathbf{F} and internal moment \mathbf{N} on a perpendicular cross section are also expanded in the basis of the triad as follows:

$$\mathbf{F} = \sum_{i=1}^3 F^i \mathbf{D}^i, \quad \mathbf{N} = \sum_{i=1}^3 N^i \mathbf{D}^i, \tag{4a}$$

$$\mathbf{f} = \sum_{i=1}^3 f^i \mathbf{D}^i, \quad \mathbf{n} = \sum_{i=1}^3 n^i \mathbf{D}^i, \tag{4b}$$

for $i = 1, 2, 3$. The constitutive relations for the unconstrained version of the Kirchhoff rod are given by:

$$N^i = a_i \left(\frac{\partial \mathbf{D}^j}{\partial s} \cdot \mathbf{D}^k - \Omega_i \right), \tag{5a}$$

$$F^i = b_i \left(\mathbf{D}^i \cdot \frac{\partial \mathbf{X}}{\partial s} - \delta_{3i} \right), \tag{5b}$$

where (i, j, k) is any cyclic permutation of $(1, 2, 3)$, i.e., $(1, 2, 3)$, $(2, 3, 1)$, and $(3, 1, 2)$. The twisting modulus of the rod is a_3 and the bending moduli are a_1 and a_2 with $a_1 = a_2$, since we assume the rod has axisymmetric material properties and a circular cross section of constant radius. The extension modulus is b_3 and the shear moduli are b_1 and b_2 . The strain twist vector is defined to be $(\Omega_1, \Omega_2, \Omega_3)$, where the intrinsic curvature is given as $\kappa = \sqrt{\Omega_1^2 + \Omega_2^2}$ and Ω_3 is the intrinsic twist whose sign determines the handedness of the rod. An open rod at a relaxed state becomes straight and untwisted when the strain twist vector is a zero vector, while the open rod becomes a helix when both intrinsic curvature and twist are nonzero. The helical pitch and radius are uniquely determined by the intrinsic curvature and twist, (κ, Ω_3) .

The constitutive relations above are derived from a variational argument of the following elastic energy penalty,

$$E = \frac{1}{2} \int_0^L \left[\sum_{i=1}^3 a_i \left(\frac{\partial \mathbf{D}^j}{\partial s} \cdot \mathbf{D}^k - \Omega_i \right)^2 + \sum_{i=1}^3 b_i \left(\mathbf{D}^i \cdot \frac{\partial \mathbf{X}}{\partial s} - \delta_{3i} \right)^2 \right] ds, \tag{6}$$

where (i, j, k) is again any cyclic permutation of $(1, 2, 3)$. In the limit as $b_i \rightarrow \infty$, we have the standard Kirchhoff rod model. See [16] for more detail. In this unconstrained Kirchhoff rod model, the penalty formulation tends to maintain the inextensibility constraint and tends to maintain that \mathbf{D}^3 is the unit tangent vector to the rod.

3. Regularized Stokes formulation

In this section we establish the exact regularized solutions of the incompressible Stokes equations in \mathbb{R}^3 to describe an elastic rod with intrinsic curvature and twist. The rod is moving in a viscous, incompressible fluid, thus its movement is driven by regularized forces and torques as defined by the Kirchhoff rod model, described in §2. To simplify the derivation, we first look at the local linear and angular velocity of the Stokes equations for a single point force and torque applied at the same point. This derivation will then be extended from the case of a single point force and torque to the case of forces and torques along the rod.

In the low Reynolds number regime, where viscous forces dominate, many methods have utilized the linearity of the Stokes equations to derive solutions in terms of fundamental solutions, Stokeslets. When the forces are concentrated along a curve in \mathbb{R}^3 , the Stokeslet solution is singular when evaluated at a point along the curve. Due to this singularity in the Stokeslet, regularization techniques have been utilized. The method of regularized Stokeslets has been previously developed and implemented to calculate the local linear velocity for the case of \mathbf{f}^b corresponding to forces only [32,33], and for the case of \mathbf{f}^b corresponding to body forces and a driving torque at a single point [33,35]. This framework is now extended to the case where the force and torque can be defined at all points along the centerline and at the orthonormal triads. In addition, the twist of the elastic rod will be captured via the local angular velocity, corresponding to the rigid rotation of the orthonormal triad.

3.1. Regularized derivation for a singular force

In the case of zero Reynolds number, we assume that the fluid is governed by the Stokes equations,

$$0 = -\nabla p + \mu \Delta \mathbf{u} + \mathbf{f}^b, \tag{7}$$

$$0 = \nabla \cdot \mathbf{u}, \tag{8}$$

where μ is the fluid viscosity, \mathbf{u} is the fluid velocity, p is the fluid pressure, and \mathbf{f}^b is the force per unit volume applied to the fluid by the immersed body. The incompressibility condition is given in Eq. (8). When the elasticity of the rod is governed by the Kirchhoff model detailed in Section 2, the rod applies force and torque to the surrounding fluid. Hence, equations of motion for the rod involve both the local linear velocity and the local angular velocity of the fluid \mathbf{w} , defined as

$$\mathbf{w} = \frac{1}{2} \nabla \times \mathbf{u}. \tag{9}$$

Deriving the regularized Stokes formulation for a point force and torque applied to the fluid, we replace \mathbf{f}^b by the regularized force and torque as follows:

$$\mathbf{f}^b(\mathbf{x}) = \mathbf{g}_o \psi_\varepsilon(\mathbf{x} - \mathbf{X}_o) + \frac{1}{2} \nabla \times \mathbf{m}_o \psi_\varepsilon(\mathbf{x} - \mathbf{X}_o), \tag{10}$$

where \mathbf{g}_o is a point force and \mathbf{m}_o is a point torque, both applied at \mathbf{X}_o . Here, \mathbf{x} may be any point in the fluid, including the point where the force and torque are being applied. For simplicity in this derivation, we assume \mathbf{g}_o and \mathbf{m}_o are constant. However, in the elastic rod applications, they depend on time and the Lagrangian parameter s . The cutoff (or blob) function ψ_ε is a radially symmetric smooth approximation to a three-dimensional delta distribution and has the property that

$$\int_{\mathbb{R}^3} \psi_\varepsilon(\mathbf{x} - \mathbf{X}_o) d\mathbf{x} = 1. \tag{11}$$

The point force or torque is spread by the cutoff function ψ_ε to a region centered at \mathbf{X}_o . The regularization parameter ε is a numerical parameter that controls the effective radius of the region where the support is concentrated [33]. Examples of three-dimensional, radially symmetric cutoff functions with infinite support include:

$$\psi_\varepsilon(r) = \frac{15\varepsilon^4}{8\pi(r^2 + \varepsilon^2)^{7/2}}, \tag{12}$$

$$\psi_\varepsilon(r) = \frac{15\varepsilon^6 \left(5 - \frac{2r^2}{\varepsilon^2}\right)}{16\pi(r^2 + \varepsilon^2)^{9/2}}, \tag{13}$$

where $r = \|\mathbf{x} - \mathbf{X}_o\|$. In Fig. 1, a graph of the cutoff function in Eq. (13) is given for different values of the regularization parameter ε . Note that as ε increases, the height of the cutoff function decreases due to the constraint that $\int_{\mathbb{R}^3} \psi_\varepsilon(\mathbf{x} - \mathbf{X}_o) d\mathbf{x} = 1$. In the limit as $\varepsilon \rightarrow 0$, we recover a Dirac delta function.

Similar to the derivation in [32], we now define two functions $G_\varepsilon(\mathbf{x})$ and $B_\varepsilon(\mathbf{x})$ as the solutions of

$$\Delta G_\varepsilon = \psi_\varepsilon(\mathbf{x}) \quad \text{and} \quad \Delta B_\varepsilon = G_\varepsilon \quad \text{in } \mathbb{R}^3, \tag{14}$$

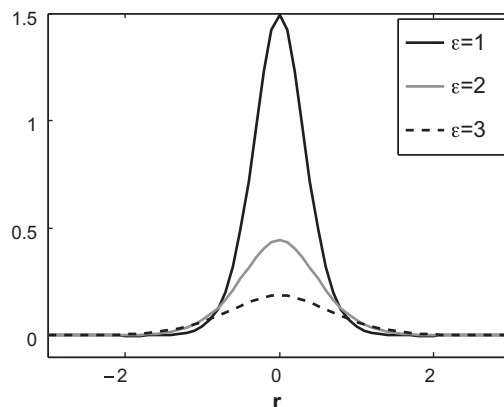


Fig. 1. Blob function given in Eq. (13) for different values of the regularization parameter ε .

where G_ε and B_ε are smooth approximations of the Green's function and the solution to the biharmonic equation, respectively. We write the regularized fundamental solution of the incompressible Stokes Eqs. (7, 8) and (10) for the local linear velocity in the form of

$$\mathbf{u} = \frac{1}{\mu} \mathbf{u}_S[\mathbf{g}_o] + \frac{1}{\mu} \mathbf{u}_R[\mathbf{m}_o], \quad (15)$$

where $\mathbf{u}_S[\mathbf{g}_o]$ and $\mathbf{u}_R[\mathbf{m}_o]$ are the regularized Stokeslet given the point force \mathbf{g}_o and the regularized rotlet given the point torque \mathbf{m}_o , respectively. They are given specifically by

$$\mathbf{u}_S[\mathbf{g}_o] = (\mathbf{g}_o \cdot \nabla) \nabla B_\varepsilon - \mathbf{g}_o G_\varepsilon, \quad (16)$$

$$\mathbf{u}_R[\mathbf{m}_o] = \frac{1}{2} \mathbf{m}_o \times \nabla G_\varepsilon. \quad (17)$$

Similarly, we can obtain the angular velocity \mathbf{w} by

$$\begin{aligned} \mathbf{w} &= \frac{1}{2} \nabla \times \mathbf{u} \\ &= \frac{1}{\mu} \mathbf{u}_R[\mathbf{g}_o] + \frac{1}{\mu} \mathbf{u}_D[\mathbf{m}_o], \end{aligned} \quad (18)$$

where the first term describes the regularized rotlet by the point force \mathbf{g}_o and the second term describes the regularized dipole by the point torque \mathbf{m}_o and they are written as

$$\mathbf{u}_R[\mathbf{g}_o] = \frac{1}{2} \mathbf{g}_o \times \nabla G_\varepsilon, \quad (19)$$

$$\mathbf{u}_D[\mathbf{m}_o] = -\frac{1}{4} [\nabla(\mathbf{m}_o \cdot \nabla G_\varepsilon) - \mathbf{m}_o \psi_\varepsilon]. \quad (20)$$

The above expressions for the linear velocity and the angular velocity are the regularized versions of the fundamental solutions of the Stokes equations when the regularized point force and torque are applied at \mathbf{X}_o . We wish to emphasize that Eqs. (15) and (18) are an exact solution for the regularized body forces as given in Eq. (10). For more details on the derivation of the linear and angular velocities, the reader is referred to the appendix in Section A.

3.2. Regularized Stokes formulation for an elastic rod with curvature and twist

We now extend this method for the incompressible Stokes equations where the elasticity of the rod is governed by the Kirchhoff model in Section 2 and the rod is immersed in the fluid and moving in time. The elastic rod Γ is given a Lagrangian description by a three-dimensional space curve $\mathbf{X}(s, t)$ and its associated orthonormal basis $\{\mathbf{D}^1(s, t), \mathbf{D}^2(s, t), \mathbf{D}^3(s, t)\}$ that indicates the amount of curvature and twist of the rod. The variable s is a material coordinate along the rod initialized as arclength and t is time. We use the force and torque balance Eqs. (3a)–(5b) described in Section 2 to describe the elastic rod Γ , which is assumed to be neutrally buoyant. Since the rod is moving in the fluid, each of the variables in these equations are now functions of s and t . Together with Eqs. (3a)–(5b), (7)–(9), the coupled system of continuous equations of the regularized Stokes formulation is as follows:

$$\mathbf{f}^b(\mathbf{x}, t) = \int_\Gamma (-\mathbf{f}(s, t)) \psi_\varepsilon(\mathbf{x} - \mathbf{X}(s, t)) ds + \frac{1}{2} \nabla \times \int_\Gamma (-\mathbf{n}(s, t)) \psi_\varepsilon(\mathbf{x} - \mathbf{X}(s, t)) ds, \quad (21a)$$

$$\frac{\partial \mathbf{X}(s, t)}{\partial t} = \mathbf{u}(\mathbf{X}(s, t), t), \quad (21b)$$

$$\frac{\partial \mathbf{D}^i(s, t)}{\partial t} = \mathbf{w}(\mathbf{X}(s, t), t) \times \mathbf{D}^i(s, t), i = 1, 2, 3. \quad (21c)$$

The evaluation point \mathbf{x} may be anywhere in \mathbb{R}^3 , including points along the rod. Eq. (21a) describes how to regularize and apply the force and torque generated by the Kirchhoff rod model to the surrounding fluid. The no-slip condition for the velocity is given in Eq. (21b), which states that the linear velocity of a material point corresponds to the local linear fluid velocity at that point. Similarly, Eq. (21c) is a no-slip condition for the angular velocity, which states that the rotation of the orthonormal triad is a rigid rotation corresponding to the angular velocity of the fluid at that point.

In the simplified derivation in Section 3.1, the body force \mathbf{f}^b is a single point force and torque applied at a point \mathbf{X}_o . In the moving rod, \mathbf{f}^b corresponds to a sum of point forces and torques distributed along the centerline $\mathbf{X}(s, t)$ of the rod, which will be discretized into M immersed boundary points. Due to the linearity of the Stokes equations, we can now extend the regularized fundamental solutions in Eqs. (15) and (18) to a superposition of fundamental solutions, corresponding to the contributions of many body forces along the elastic rod, all defined by Eq. (21a). There are a few important aspects of

the regularized Stokes formulation that we wish to emphasize. The original derivation of the Kirchhoff rod assumes a rod thickness that is much smaller than the rod length. In this method, we are only tracking a space curve corresponding to the centerline. However, the regularization parameter ε that is introduced for computational reasons, can be interpreted as the radial extent of the rod cross-section where the forces are exerted. In this sense, the regularization parameter can be given a physical meaning. Additionally, due to the regularization of the forces and torques applied to the fluid via the blob function, we obtain a finite velocity everywhere, including on the space curve that represents the rod. Moreover, the solution we obtain is incompressible everywhere. The numerical algorithm, detailed in the next section, will describe the discretization and calculation of the force and torque, as well as the calculation of the local linear and angular velocity.

4. Numerical method for Stokes formulation

In this section, we describe the numerical scheme that we use to solve the equations of motion in Eqs. (7, 8) together with Eq. (10), when the force and torque are given by Eqs. (3a)–(5b) and (21a), subject to the no-slip conditions given in Eqs. (21b) and (21c). We discretize the rod centerline into M immersed boundary points by letting Δs be a fixed uniform interval of the Lagrangian parameter s . Each material point on the rod will be given a point index k , such that $s_k = k\Delta s$, for $k = 1, 2, \dots, M$. The Lagrangian variables \mathbf{X} , \mathbf{D}^1 , \mathbf{D}^2 , \mathbf{D}^3 , \mathbf{F} , \mathbf{N} , \mathbf{f} , and \mathbf{n} will be defined at points s_k for integer values of k , and for such variables we shall use the notation $\mathbf{X}_k = \mathbf{X}(k\Delta s)$, etc. The variables \mathbf{X} , \mathbf{D}^1 , \mathbf{D}^2 , \mathbf{D}^3 , \mathbf{F} , and \mathbf{N} will also be defined at $s_{k+\frac{1}{2}}$ for half-integer values, where k is restricted to integer values. The body force in Eq. (21a) will be discretized as follows,

$$\mathbf{f}^b(\mathbf{x}) = \sum_{k=1}^M -\mathbf{f}_k \Delta s \psi_\varepsilon(\mathbf{x} - \mathbf{X}_k) + \frac{1}{2} \nabla \times \sum_{k=1}^M -\mathbf{n}_k \Delta s \psi_\varepsilon(\mathbf{x} - \mathbf{X}_k), \quad (22)$$

where the summation is over each of the immersed boundary points. The curl is discretized using a standard central difference approximation, see [16] for details. Note that $-\mathbf{f}_k \Delta s$ and $-\mathbf{n}_k \Delta s$ correspond to the terms \mathbf{g}_o and \mathbf{m}_o , respectively, from the derivation of the simplified case in Section 3.1.

We use a slight perturbation of a given configuration for the initial configuration of the rod, which is detailed for each of the numerical examples that are presented in Section 6. Given a configuration of the rod \mathbf{X} and $\{\mathbf{D}^1, \mathbf{D}^2, \mathbf{D}^3\}$, and given a particular cutoff function ψ_ε :

1. Compute the force and moment that are transmitted across the section of the rod using a discretization of Eqs. (5a) and (5b)

$$F_{k+\frac{1}{2}}^i = b_i \left(\mathbf{D}_{k+\frac{1}{2}}^i \cdot \frac{\mathbf{X}_{k+1} - \mathbf{X}_k}{\Delta s} - \delta_{3i} \right), \quad (23)$$

$$N_{k+\frac{1}{2}}^1 = a_1 \left(\frac{\mathbf{D}_{k+1}^2 - \mathbf{D}_k^2}{\Delta s} \cdot \mathbf{D}_{k+\frac{1}{2}}^3 - \Omega_1 \right), \quad (24)$$

$$N_{k+\frac{1}{2}}^2 = a_2 \left(\frac{\mathbf{D}_{k+1}^3 - \mathbf{D}_k^3}{\Delta s} \cdot \mathbf{D}_{k+\frac{1}{2}}^1 - \Omega_2 \right), \quad (25)$$

$$N_{k+\frac{1}{2}}^3 = a_3 \left(\frac{\mathbf{D}_{k+1}^1 - \mathbf{D}_k^1}{\Delta s} \cdot \mathbf{D}_{k+\frac{1}{2}}^2 - \Omega_3 \right). \quad (26)$$

The force and torque vectors may be expressed in the basis of triads:

$$\mathbf{F}_{k+\frac{1}{2}} = \sum_{i=1}^3 F_{k+\frac{1}{2}}^i \mathbf{D}_{k+\frac{1}{2}}^i, \quad \mathbf{N}_{k+\frac{1}{2}} = \sum_{i=1}^3 N_{k+\frac{1}{2}}^i \mathbf{D}_{k+\frac{1}{2}}^i. \quad (27)$$

The orthonormal triad $(\mathbf{D}_{k+\frac{1}{2}}^1, \mathbf{D}_{k+\frac{1}{2}}^2, \mathbf{D}_{k+\frac{1}{2}}^3)$ can be evaluated at the point $s_{k+\frac{1}{2}}$ as follows:

$$\mathbf{D}_{k+\frac{1}{2}}^i = \sqrt{A} \mathbf{D}_k^i, \quad (28)$$

where $i = 1, 2, 3$ and A is an orthogonal matrix which maps the triad \mathbf{D}_k^i to the triad $\mathbf{D}_{k+\frac{1}{2}}^i$ ($i = 1, 2, 3$) defined by

$$A = \sum_{i=1}^3 \mathbf{D}_{k+\frac{1}{2}}^i (\mathbf{D}_k^i)^T, \quad (29)$$

where T stands for the transpose of a matrix. Here A is a rotation about a certain axis through a certain angle θ and \sqrt{A} is the principal square root of the matrix A , which is a rotation about that same axis by half the angle. For a more detailed description, see [16].

2. Compute force and torque exerted by the fluid at the material point s_k by discretizing Eqs. (3a) and (3b) as follows:

$$-\mathbf{f}_k = \frac{\mathbf{F}_{k+\frac{1}{2}} - \mathbf{F}_{k-\frac{1}{2}}}{\Delta S}, \quad (30)$$

$$-\mathbf{n}_k = \frac{\mathbf{N}_{k+\frac{1}{2}} - \mathbf{N}_{k-\frac{1}{2}}}{\Delta S} + \frac{1}{2} \left(\frac{\mathbf{X}_{k+1} - \mathbf{X}_k}{\Delta S} \times \mathbf{F}_{k+\frac{1}{2}} + \frac{\mathbf{X}_k - \mathbf{X}_{k-1}}{\Delta S} \times \mathbf{F}_{k-\frac{1}{2}} \right). \quad (31)$$

3. Compute the local linear fluid velocity at any point \mathbf{x} by:

$$\mathbf{u}(\mathbf{x}) = \frac{1}{\mu} \sum_{k=1}^M \mathbf{u}_S[-\mathbf{f}_k \Delta S] + \frac{1}{\mu} \sum_{k=1}^M \mathbf{u}_R[-\mathbf{n}_k \Delta S], \quad (32)$$

where $\mathbf{u}_S[-\mathbf{f}_k \Delta S]$ and $\mathbf{u}_R[-\mathbf{n}_k \Delta S]$ are the regularized Stokeslet and rotlet from the point force and torque applied at \mathbf{X}_k , respectively. See the appendix for the detailed formulation.

4. Compute the local angular velocity of the fluid at any point \mathbf{x} by:

$$\mathbf{w}(\mathbf{x}) = \frac{1}{\mu} \sum_{k=1}^M \mathbf{u}_R[-\mathbf{f}_k \Delta S] + \frac{1}{\mu} \sum_{k=1}^M \mathbf{u}_D[-\mathbf{n}_k \Delta S], \quad (33)$$

where $\mathbf{u}_R[-\mathbf{f}_k \Delta S]$ and $\mathbf{u}_D[-\mathbf{n}_k \Delta S]$ are the regularized rotlet and dipole from the point force and torque applied at \mathbf{X}_k , respectively. See the appendix for the detailed formulation.

5. Update the position of the rod and triads: Let the superscript n be the time-step index, such that \mathbf{X}_k^n denotes the position of the rod immersed in the fluid at time $t = n\Delta t$, where Δt is the time-step duration. Once the fluid velocity \mathbf{u} and the angular fluid velocity \mathbf{w} at the immersed boundary point \mathbf{X}_k^n are known, we define

$$\mathbf{X}_k^{n+1} = \mathbf{X}_k^n + \mathbf{u}(\mathbf{X}_k^n) \Delta t, \quad (34)$$

$$(\mathbf{D}_k^i)^{n+1} = R \left(\frac{\mathbf{w}(\mathbf{X}_k^n)}{|\mathbf{w}(\mathbf{X}_k^n)|}, |\mathbf{w}(\mathbf{X}_k^n)| \Delta t \right) (\mathbf{D}_k^i)^n, \quad (35)$$

where $i = 1, 2, 3$ and $k = 1, \dots, M$. $R(\mathbf{e}, \theta)$ is the orthogonal matrix that describes a rotation through an angle about the axis of the unit vector \mathbf{e} and the formulation is explicitly given by

$$R(\mathbf{e}, \theta) = (\cos \theta) I + (1 - \cos \theta) \mathbf{e} \mathbf{e}^T + (\sin \theta) (\mathbf{e} \times), \quad (36)$$

where I is the 3×3 identity matrix and $(\mathbf{e} \times)$ is the antisymmetric 3×3 matrix defined by $(\mathbf{e} \times) \mathbf{v} = \mathbf{e} \times \mathbf{v}$ for any \mathbf{v} .

We update the location of the rod and orthonormal triad in step #5 above using no-slip conditions. Specifically, in Eq. (34), we are using Euler method, which is first order accurate. In this step, one could easily substitute a higher order explicit method, such as the Runge–Kutta method.

5. Generalized immersed boundary (gIB) method

We summarize the gIB method in order to compare its numerical results with those from the regularized Stokes formulation described in Sections 3 and 4. For further details, see Lim et al. [16] and Lim [17]. In the gIB formulation, we employ two different types of variables, Eulerian and Lagrangian forms. The former is used to describe the fluid motion on fixed Cartesian coordinates, whereas the latter is used to describe the motion of the structure immersed in that fluid. The fluid and the immersed structure defined on the two different coordinate systems interact with each other via a C^1 -function approximated smoothly to a three-dimensional delta function. The gIB method has been developed to model an elastic rod immersed in a fluid, using the unconstrained Kirchhoff rod theory. The key features of the gIB formulation, as an extension of the standard IB method, are that elastic rods apply both force and torque to the surrounding fluid; and the rod moves according to the local linear velocity and rotates according to the local angular velocity.

In order to compare to the regularized Stokes formulation, we use the same description for the rod as detailed in the previous sections, with $\mathbf{X}(s, t)$ as the centerline of the rod and the associated orthonormal basis $\{\mathbf{D}^1(s, t), \mathbf{D}^2(s, t), \mathbf{D}^3(s, t)\}$. The Eulerian variables are functions of (\mathbf{x}, t) , where $\mathbf{x} = (x_1, x_2, x_3)$ is the fixed Cartesian coordinate. Together with the torque and force balance given in Eqs. (3a)–(5b), the coupled system of continuous equations of the gIB method is as follows:

$$\rho \left(\frac{\partial \mathbf{u}}{\partial t} + \mathbf{u} \cdot \nabla \mathbf{u} \right) = -\nabla p + \mu \nabla^2 \mathbf{u} + \mathbf{f}^b, \quad (37a)$$

$$\nabla \cdot \mathbf{u} = 0, \quad (37b)$$

$$\mathbf{f}^b = \int (-\mathbf{f}(s, t)) \delta_c(\mathbf{x} - \mathbf{X}(s, t)) ds + \frac{1}{2} \nabla \times \int (-\mathbf{n}(s, t)) \delta_c(\mathbf{x} - \mathbf{X}(s, t)) ds, \quad (37c)$$

$$\frac{\partial \mathbf{X}(s, t)}{\partial t} = \mathbf{U}(s, t) = \int \mathbf{u}(\mathbf{x}, t) \delta_c(\mathbf{x} - \mathbf{X}(s, t)) d\mathbf{x}, \quad (37d)$$

$$\mathbf{W}(s, t) = \frac{1}{2} \int (\nabla \times \mathbf{u}) \delta_c(\mathbf{x} - \mathbf{X}(s, t)) d\mathbf{x}, \quad (37e)$$

$$\frac{\partial \mathbf{D}^i(s, t)}{\partial t} = \mathbf{W}(s, t) \times \mathbf{D}^i(s, t), i = 1, 2, 3. \quad (37f)$$

The incompressible Navier–Stokes equations are given in Eqs. (37a) and (37b), where ρ is the fluid density. When the above equations are discretized, the Eulerian variables $\mathbf{u}(\mathbf{x}, t)$, $p(\mathbf{x}, t)$, and $\mathbf{f}^b(\mathbf{x}, t)$ are now defined only at fixed Cartesian grid points $\mathbf{x} = (x_1, x_2, x_3)$. The Lagrangian variables are the centerline \mathbf{X} , the orthonormal triads \mathbf{D} , the locally averaged linear velocity at the centerline \mathbf{U} , and the locally averaged angular velocity at the centerline \mathbf{W} .

The interaction of the rod with the fluid is described by Eqs. (37c)–(37e). These interaction equations connect the Lagrangian and Eulerian variables via a three-dimensional smoothed Dirac delta function $\delta_c(\mathbf{x})$, where c is a physical parameter that is proportional to the effective thickness of the rod. We choose $\delta_c(\mathbf{x})$ as

$$\delta_c(\mathbf{x}) = \frac{1}{c^3} \phi\left(\frac{x_1}{c}\right) \phi\left(\frac{x_2}{c}\right) \phi\left(\frac{x_3}{c}\right), \quad (38)$$

where ϕ is a bell function with compact support:

$$\phi(r) = \begin{cases} \frac{3-2|r|+\sqrt{1+4|r|-4r^2}}{8} & |r| \leq 1, \\ \frac{5-2|r|-\sqrt{-7+12|r|-4r^2}}{8} & 1 \leq |r| \leq 2, \\ 0 & |r| \geq 2. \end{cases}$$

Note that $\delta_c(\mathbf{x} - \mathbf{X})$ is a continuous function of \mathbf{x} with continuous first derivatives and with support equal to a cube of edge $4c$ centered on \mathbf{X} . Eq. (37c) shows how to apply the force and torque of the rod to the surrounding fluid. Eq. (37d) is the no-slip condition which states that the velocity of an immersed boundary point on the rod coincides with the locally averaged fluid velocity evaluated at that point, and Eqs. (37e) and (37f) imply that the triad at each point of the rod rotates at the locally averaged angular velocity of the fluid.

All gIB simulations will be completed in a 3-dimensional periodic box where the Eulerian variables will be set on a fixed Cartesian grid of constant meshwidth h that consists of $N \times N \times N$ grid points. The Lagrangian variables have the same discretization as described in the Stokes formulation, with the rod having spatial step size Δs and the rod is discretized into M immersed boundary points. The finite difference method described in steps #1–2 of the numerical algorithm in Section 4 is employed to solve for the force and torque equations in the gIB method. The force and torque are spread to the Cartesian grid points using a discretized version of Eq. (37c). The discretized incompressible Navier–Stokes equation are then solved at each of the Cartesian grid points using the fast Fourier transform. The immersed boundary points are then updated using the locally averaged fluid velocity and the orientation of the orthonormal triad is updated using the locally averaged angular velocity. For more details on the numerical algorithm used for the gIB method, see [16,17].

6. Numerical examples

We validate the regularized Stokes formulation for an elastic rod immersed in a viscous fluid developed in Section 3, using the numerical algorithm detailed in Section 4. Test cases, including open and closed elastic rods, are compared to established results of equilibrium configurations in elastic rod theory. Additionally, we compare the regularized Stokes formulation to the gIB method, summarized in Section 5, in the low Reynolds number regime. In order to compare the gIB method and regularized Stokes formulation, we focus on computational efficiency, equilibrium configurations, and energy profiles as the rod is moving and interacting with the fluid.

The computational parameters for both the gIB method and regularized Stokes formulation are summarized in Table 1. In order to compare the computational efficiency of these two methods, the Lagrangian discretization of the rod is kept constant for each type of rod and the time step is fixed across all simulations. Since the gIB method has an Eulerian discretization for the fluid domain, a periodic box, these computational parameters are also detailed in Table 1. We also choose a sufficiently large periodic box so that the interactions with the periodic copies are insignificant (doubling of the box results in energy profiles that vary by less than 4% on average). For comparison, the Reynolds number Re , defined as

$$Re = \frac{\rho UL}{\mu}, \quad (39)$$

is fixed at 10^{-4} where the length scale L is the length of the rod, U is the maximum velocity of the fluid, and the values used for ρ and μ are reported in Table 1. The blob or cutoff function used in all simulations of the regularized Stokes formulation is given in Eq. (12).

Table 1

Computational parameters for open and closed rod (sec = seconds).

| | Open | Closed |
|---|--------------------------|--------------------------|
| <i>Stokes formulation and gIB method</i> | | |
| Unstressed rod, L (μm) | 6 | 15.708 |
| Immersed Boundary points, M | 76 | 200 |
| Meshwidth for rod, Δs (μm) | 0.0785 | 0.0785 |
| Time step, Δt (s) | 1×10^{-6} | 1×10^{-6} |
| Fluid viscosity, μ ($\text{g } \mu\text{m}^{-1} \text{s}^{-1}$) | 1×10^{-6} | 1×10^{-6} |
| <i>Regularized Stokes formulation</i> | | |
| Regularization parameter, ε (μm) | $5\Delta s - 8\Delta s$ | $3\Delta s - 6\Delta s$ |
| <i>gIB Method</i> | | |
| Length of fluid domain (μm) | 10 | 10 |
| Cartesian grid size ($N \times N \times N$) | $64 \times 64 \times 64$ | $64 \times 64 \times 64$ |
| Meshwidth for fluid, h (μm) | $2\Delta s$ | $2\Delta s$ |
| Delta function parameter, c (μm) | $2\Delta s$ | $2\Delta s$ |
| Fluid density, ρ ($\text{g } \mu\text{m}^{-3}$) | 1×10^{-12} | 1×10^{-12} |
| Reynolds number, $\mathcal{R}e$ | 10^{-4} | 10^{-4} |

Table 2

Material parameters for open and closed rods. These parameters are the same for the Stokes formulation and the gIB method (sec = seconds).

| | Open | Closed |
|--|----------------------|----------------------|
| Bending modulus, $a = a_1 = a_2$ ($\text{g } \mu\text{m}^3 \text{s}^{-2}$) | 3.5×10^{-3} | 3.5×10^{-3} |
| Twist modulus, a_3 ($\text{g } \mu\text{m}^3 \text{s}^{-2}$) | 3.5×10^{-3} | 3.5×10^{-3} |
| Shear modulus, $b = b_1 = b_2$ ($\text{g } \mu\text{m}^3 \text{s}^{-2}$) | 8.0×10^{-1} | 8.0×10^{-1} |
| Stretch modulus, b_3 ($\text{g } \mu\text{m}^3 \text{s}^{-2}$) | 8.0×10^{-1} | 8.0×10^{-1} |
| Perturbation parameter, ξ | 0.0001 | 1 |
| Strain twist vector, $(\Omega_1, \Omega_2, \Omega_3)$ (μm^{-1}) | Varied | Varied |

The material parameters for the open and closed rods are summarized in Table 2. It is noted that material properties, along with intrinsic properties, will determine the stability of an elastic rod. Since we are comparing the regularized Stokes formulation with the gIB method, these parameters will be the same for both cases. We wish to emphasize that the time steps and material parameters chosen ensure (within 1% relative error) that the rod tends to maintain the inextensibility constraint and that the \mathbf{D}^3 is aligned with the tangent vector, via the elastic energy penalty in Eq. (6). In the following subsections, we will focus on the rod stability as the intrinsic curvature and twist are varied and provide an application of the regularized Stokes formulation at the end of this section.

6.1. Open elastic rod

As a benchmark comparison, we investigate the dynamics of an open elastic rod immersed in a viscous fluid. A straight rod is considered and represented by a three-dimensional space curve and an orthonormal triad, $\{\mathbf{X}(s, t), \mathbf{D}^1(s, t), \mathbf{D}^2(s, t), \mathbf{D}^3(s, t)\}$. Both ends of the rod freely move through the fluid. The initial configuration of the rod will be a perturbation of the straight rod as follows:

$$\mathbf{X}(s) = (0, 0, (1 + \xi)s), \quad (40)$$

$$\mathbf{D}^1(s) = (1, 0, 0), \quad (41)$$

$$\mathbf{D}^2(s) = (0, \cos(\xi), -\sin(\xi)), \quad (42)$$

$$\mathbf{D}^3(s) = (0, \sin \xi, \cos \xi), \quad (43)$$

where the rod is given a strain twist vector, $\{\Omega_1, \Omega_2, \Omega_3\}$, that determines the intrinsic curvature and torsion of the rod. The perturbation of the rod is controlled by the parameter ξ and is chosen to correspond with previous gIB simulations [17]. Since an equilibrium configuration of the rod is $\mathbf{X}(s) = (0, 0, s)$, the perturbation is used to ensure the rod is not initialized in the equilibrium configuration. We solve the discretized version of the regularized Stokes formulation, as outlined in Section 4. Since this is an open rod, the internal force and moment boundary conditions are prescribed as follows:

$$\mathbf{F}_{1/2} = \mathbf{F}_{M+1/2} = \mathbf{0}, \mathbf{N}_{1/2} = \mathbf{N}_{M+1/2} = \mathbf{0}, \quad (44)$$

where M is the total number of immersed boundary points along the rod. When the rod is initialized as a perturbation of a straight rod, it will continue to move and interact with the surrounding fluid until it reaches its equilibrium configuration, as defined by the strain twist vector.

According to the Kirchhoff theory for elastic rods, any perturbed open rod whose strain twist vector is set equal to zero, $(\Omega_1, \Omega_2, \Omega_3) = (0, 0, 0)$, will relax to a stable equilibrium state that is a straight, untwisted rod [41,42]. Numerical results for this strain twist vector are not shown, but were verified and match the results established by elastic rod theory. Through linear stability analysis, it has been shown that if $\kappa > 0$ and the twist is greater than a critical twist value, a straight rod will become unstable and bifurcate into a stable helix configuration [3]. (The critical twist value depends on the material parameters of the rod, as well as the strain twist vector [4].) Geometric properties of this new helix equilibrium configuration, such as the number of turns along the rod q , can be determined as

$$q = \frac{\Omega_3 L}{2\pi}, \quad (45)$$

where Ω_3 is the intrinsic twist (or torsion) of the rod and L is the length of the rod. In Fig. 2, representative results for the regularized Stokes formulation are shown for two different strain twist vectors, where the configurations of the rod are at increments of 0.001 s. In these cases, the twist is high enough to cause the rod to go from its initial configuration to an equilibrium configuration that is a stable helix. Verifying the results with elastic rod theory, it can be seen for the simulated 6 μm rod in Fig. 2 that the top panel has $q = 1.5$ turns when $\Omega_3 = \pi/2$ and the bottom panel has $q = 3$ turns when $\Omega_3 = \pi$. The configuration at each of the time points also matches the gIB results when solving the Navier–Stokes equations on a periodic domain.

We also examined the time profile of the energy to understand and verify how the rod is moving and interacting with the fluid as it reaches its equilibrium configuration. The classical results of elastic rod theory do not capture the interaction of the rod with the fluid, therefore we compare the energy profiles to those obtained from the gIB method that is described in Sec-

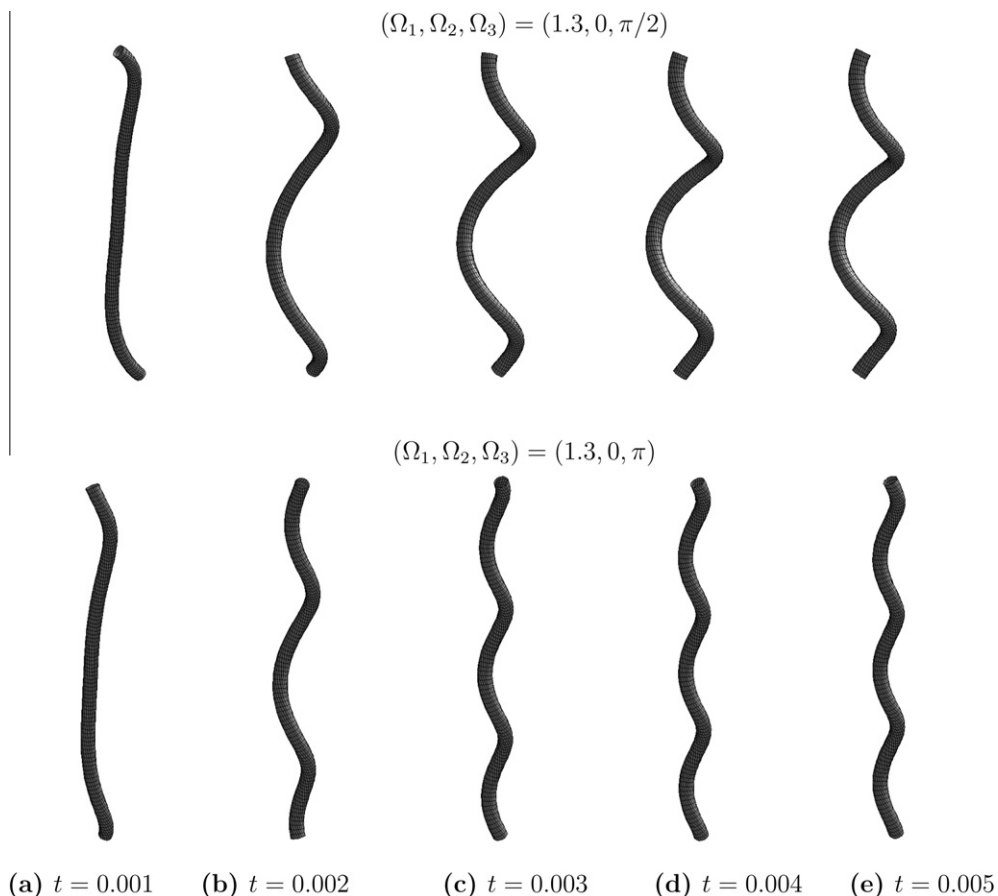


Fig. 2. Results of regularized Stokes formulation where the open rod is initialized as a perturbation of a straight rod with nonzero intrinsic curvature and twist. The top and bottom rows correspond to rods with strain twist vector's $(1.3, 0, \pi/2)$ and $(1.3, 0, \pi)$, respectively. In both rows, going from left to right, (a)–(e) represents the time profiles between $t = 0.001$ and $t = 0.005$ s, where each graph increments by 0.001 s. The regularization parameter used is $\varepsilon = 6\Delta s$.

tion 5. For comparison, energy profiles are shown in Fig. 3 for strain-twist vector $(\Omega_1, \Omega_2, \Omega_3) = (1.3, 0, \pi)$, with time dependent configuration corresponding to the bottom row of Fig. 2. Each plot displays five curves, one corresponding to the result from the gIB method where δ_c is given in Eq. (38), and the rest correspond to the results from the Stokes formulation for four different values of ε . Here, the energy profiles are calculated as the discretized version of Eq. (6) and the units of energy are kT . Here, k is the Boltzmann's constant (Joules per Kelvin) and T is the temperature in degrees Kelvin, set to room temperature. The Stokes formulation uses an infinite support blob given in Eq. (12), that spreads the majority of the force and torque in a sphere of radius ε around the given point. We choose to vary the regularization parameter ε from $5\Delta s$ to $8\Delta s$. Note that in Fig. 3(a)–(d), the regularized Stokes formulation profiles follow the same trends as the gIB method. Additionally, for this set of parameters, the regularized Stokes formulation matches the gIB method curve for the case of $\varepsilon = 6\Delta s$. Recall that in the gIB method, the discrete delta function has cubic compact support of length $4c = 8\Delta s$. The regularized Stokeslet blob has infinite support and is radial, so it is difficult to make a direct comparison. However, the regularization parameter of $\varepsilon = 6\Delta s$ is consistent with the corresponding size in the gIB method. The fluid domain is different in the two methods, thus we have chosen a sufficiently large periodic domain for the gIB method to eliminate any significant interactions with periodic copies. Since the governing equations of the fluid are different for the two methods, we do not expect the curves to match exactly. However, the results verify that the energy profiles of the regularized Stokes formulation are similar in magnitude and trend to the gIB method as well as the overall shape of the equilibrium configuration. As expected, Fig. 3 shows that the bending energy in (a), twist energy in (c), and total energy in (d) decrease monotonically from the initial amount stored in the rod down to zero as the rod reaches its equilibrium configuration. As the rod is interacting with the fluid, the kinetic energy in (b) increases at first, and then decreases, which implies that the rod moves quickly initially and then slows down. These trends in the energy profiles are seen in both the regularized Stokes formulation and the gIB method. Although the energy penalty function seen in Eq. (6) includes shearing and stretching energy terms, they are small enough to be negligible.

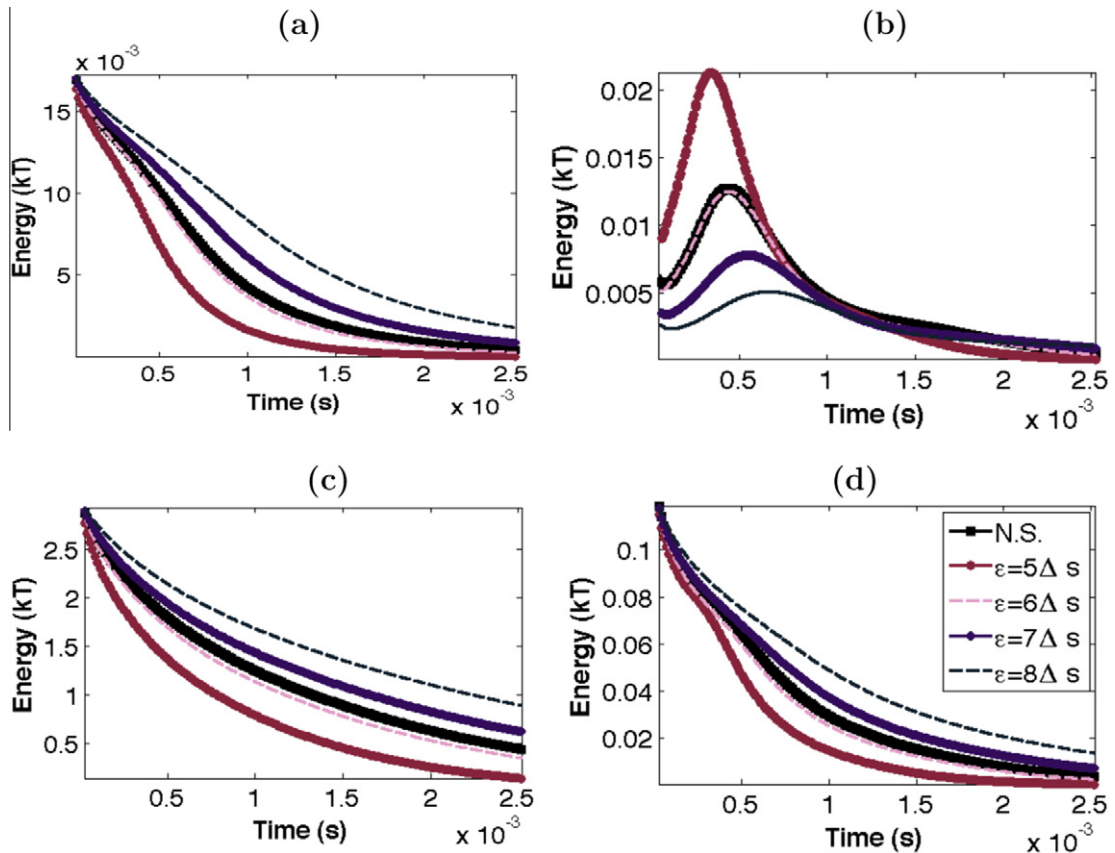


Fig. 3. The energy profiles are as follows: (a) Bending energy, (b) Kinetic energy, (c) Twisting energy, (d) Total energy. Each panel displays five curves: one for the Navier Stokes case with a virtual radius of $c = 2\Delta s$ (solid black line). The other curves correspond to simulations of the regularized Stokes formulation for $\varepsilon = 5\Delta s, 6\Delta s, 7\Delta s,$ and $8\Delta s$, where ε is the regularization parameter of the blob function given in Eq. (12). For the energy profiles shown, the strain twist vector is: $(\Omega_1, \Omega_2, \Omega_3) = (1.3, 0, \pi)$. In each of the plots, the x-axis corresponds to the time in seconds (s) and the y-axis corresponds to the Energy (kT), where k is the Boltzmann's constant (Joules per Kelvin) and T is the temperature in degrees Kelvin, set to room temperature.

6.2. Closed elastic rod

As a second benchmark comparison, we study the dynamics of an intrinsically curved and twisted closed elastic rod immersed in a viscous fluid. The initial configuration of the rod is set to a sinusoidal perturbation of an equilibrium solution of Eqs. (3a) and (3b) in the absence of any applied forces and moments. This equilibrium configuration takes the form of a circular rod in a horizontal plane and is untwisted initially. The rod will have length $L = 2\pi r_0$, which is the circumference of the unstressed rod with radius r_0 , where $0 \leq s \leq 2\pi r_0$. The rod is given by

$$\mathbf{X}(s) = r_0 \mathbf{r}\left(\frac{s}{r_0}\right), \quad (46)$$

$$\mathbf{D}^1(s) = \cos\left(\xi \sin\frac{s}{r_0}\right) \mathbf{z} + \sin\left(\xi \sin\frac{s}{r_0}\right) \mathbf{r}\left(\frac{s}{r_0}\right), \quad (47)$$

$$\mathbf{D}^2(s) = -\sin\left(\xi \sin\frac{s}{r_0}\right) \mathbf{z} + \cos\left(\xi \sin\frac{s}{r_0}\right) \mathbf{r}\left(\frac{s}{r_0}\right), \quad (48)$$

$$\mathbf{D}^3(s) = \theta\left(\frac{s}{r_0}\right), \quad (49)$$

where ξ is the perturbation parameter and (r, θ, z) are cylindrical coordinates with unit vectors $\{\mathbf{r}(\theta), \theta(\theta), \mathbf{z}\}$. The values for the length L and perturbation parameter ξ , along with the material parameters of the rod used for the simulations are given in Table 2. We solved the discretized version of the regularized Stokes formulation, as outlined in Section 4. Since this is a closed rod, assuming that $\mathbf{X}_1 = \mathbf{X}_{M+1}$, where M is the total number of immersed boundary points along the rod, periodic boundary conditions are used for the force and moment. When the rod is initialized as a perturbation of a closed circular rod, it will continue to move and interact with the surrounding fluid until it reaches its equilibrium configuration, as defined by the strain twist vector.

In Fig. 4, the configurations for the regularized Stokes formulation are given for two different intrinsic strain twist vectors. In both cases, the closed rod reaches its coiled configuration in around 0.1 s. Note that this is a much longer time scale than for the open rod to reach its helical equilibrium configuration. The closed rod does not have free ends and its motion is confined to a closed form, which elongates the time period to reach a stable equilibrium configuration. In contrast, the linear rod has two ends free to move through the fluid, which makes the rod easier to deform into a helix, as prescribed by the energy minimum configuration. In these plots, the fluid markers were initiated on the outside of the closed rod. As the rod is moving, the fluid markers give insight into how the fluid is moving close to the rod. Similar to the results of the gIB in [16], the rod becomes unstable, writhes, and starts to buckle. The ring or closed rod then forms loops back on itself until it reaches a stable coiled configuration. The achieved equilibrium configurations in Fig. 4 using the regularized Stokes formulation are more coiled in the top panel for the case of intrinsic twist $\Omega_3 = 0.6$ and less coiled in the bottom panel for the case of $\Omega_3 = 0.5$.

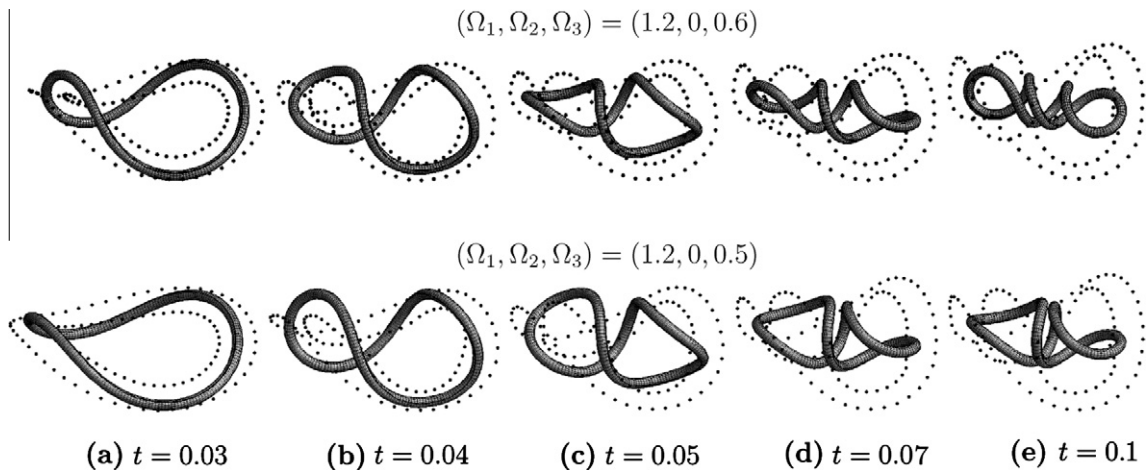


Fig. 4. Configurations for the regularized Stokes formulation where the rod is initialized as a perturbation of a circular, closed rod in a horizontal plane. The top and bottom rows correspond to rods with intrinsic strain twist vectors $(\Omega_1, \Omega_2, \Omega_3) = (1.2, 0, 0.6)$ and $(\Omega_1, \Omega_2, \Omega_3) = (1.2, 0, 0.5)$, respectively. In both rows, going from left to right, (a)–(e) represents the time profiles between $t = 0.03$ and $t = 0.1$ s. The value of regularization parameter is given as $\varepsilon = 4\Delta s$. Two layers of fluid markers (dots) are spread around the circular rod initially.

We also compared the energy profiles between the regularized Stokes formulation and the gIB method. Similar to the results for the open rod above, we fix the compact support of the δ_c function to be $c = 2\Delta s$ for the gIB (Navier–Stokes) simulations and we vary the regularization parameter of the Stokes formulation from $\varepsilon = 3\Delta s$ to $6\Delta s$. Once again, since we are comparing methods with different governing equations, we wish only to verify that the energy profiles are on the same order of magnitude and follow the same trends. The results for the energy profiles are shown in Fig. 5 for a closed elastic rod with intrinsic twist that interacts with the surrounding fluid. These profiles correspond to the configuration in the bottom panel of Fig. 4. The instability due to the value of the intrinsic twist causes the closed rod to writhe in the fluid. As this writhing and coiling occurs, the kinetic energy that is stored in the closed rod decreases to zero as shown in Fig. 5(b). Additionally, the bending and total energy, shown in Fig. 5(a) and (d), respectively, also approach zero. The stretching energy profile in Fig. 5(c) increases due to the coiled equilibrium configuration. Note that the energy profiles for the regularized Stokes formulation are in the range of those calculated by the gIB method.

6.3. Computation time

In order to study the computational efficiency of our method based on the regularized Stokes formulation, we compare the computation time to the gIB method. In both methods, the component that solves the force and torque balance on the cross section of a rod is the same. The major difference is in how the velocity is computed. In the regularized Stokes formulation, we use a superposition of fundamental solutions along the rod centerline, given in Eqs. (32) and (33), to compute the velocity. In contrast, for the gIB method, we solve for the velocity on the underlying Cartesian fluid grid and then interpolate it to the locations of the rod. The regularized Stokes formulation solves the Stokes equations in \mathbb{R}^3 and the gIB method solves the Navier Stokes equations ($Re \sim 10^{-4}$) on a periodic domain. For the gIB computations, we use the coarsest Cartesian grid that was shown to be stable in previous studies [16,17]. We also choose a sufficiently large periodic box so that the interactions with the periodic copies are negligible (doubling of the box results in energy profiles that vary by less than 4% on average). Both methods were coded in Fortran 90, compiled using pgf90, and they were run on the oneSIS cluster at the Center for Computational Science at Tulane University.

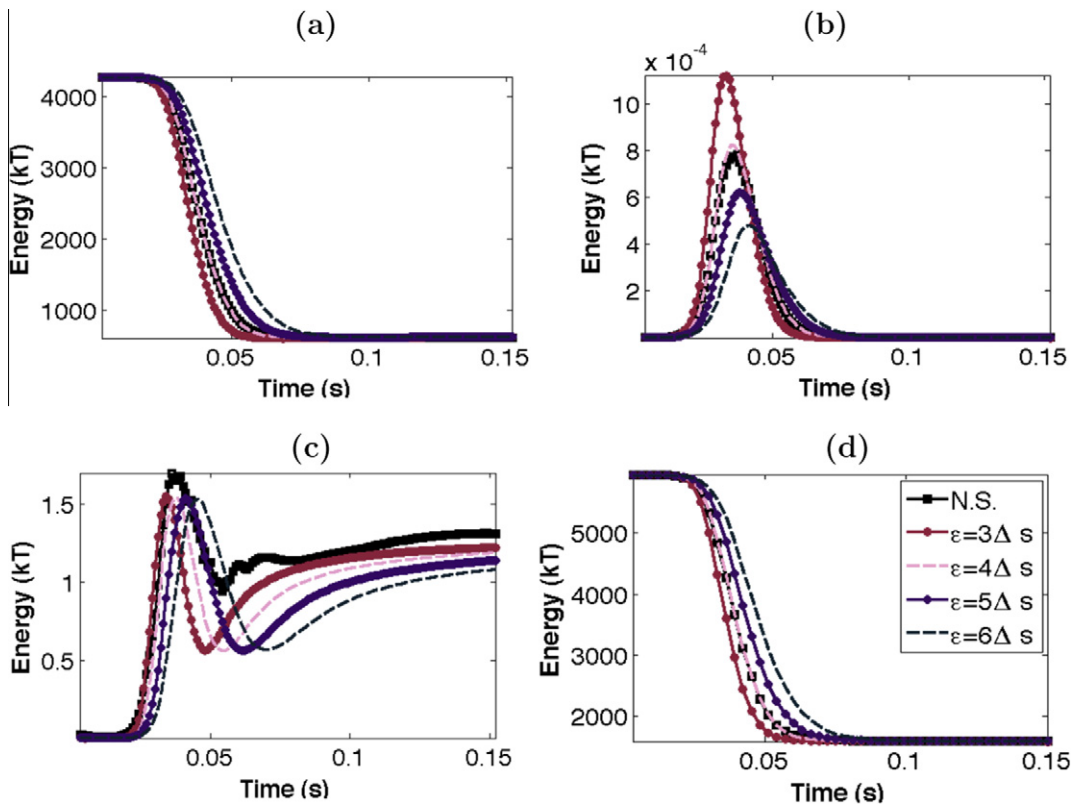


Fig. 5. The energy profiles are as follows: (a) Bending energy, (b) Kinetic energy, (c) Stretching energy, (d) Total energy. In each of the plots, there are 5 curves shown: one for the Navier Stokes gIB method with a virtual radius of $c = 2\Delta s$ (solid black line) and the other lines correspond to the simulations of the regularized Stokes formulation for $\varepsilon = 3\Delta s, 4\Delta s, 5\Delta s,$ and $6\Delta s$, where ε is the regularization parameter of the blob function given in Eq. (12). For the energy profiles shown, the strain twist vector is set to $(\Omega_1, \Omega_2, \Omega_3) = (1.2, 0, 0.5)$. In each of the plots, the x-axis corresponds to the time in seconds (s) and the y-axis corresponds to the Energy (kT), where k is the Boltzmanns constant (Joules per Kelvin) and T is the temperature in degrees Kelvin, set to room temperature. (The energy profiles correspond to a discretized version of Eq. (6)).

Table 3 shows the results of the comparison of these two methods for the case of a closed rod whose equilibrium configuration is a twisted ring. The rod is initialized as a circular tube with strain twist vector $\{\Omega_1, \Omega_2, \Omega_3\} = \{1.2, 0, 0.6\}$ and evolves in time to reach its equilibrium configuration. In both methods, the simulations were run for the same number of time steps until the rod reached the desired equilibrium configuration. The same number of immersed boundary points and fluid marker points were used in the comparison. As shown in the table, the regularized Stokes formulation runs more than 12 times faster than the gIB method when using 200 immersed boundary points. Similar times were observed for the case of an open rod as well as other cases of the closed rod (results not shown). We note that as the number of immersed boundary points increases, the factor of speed up is not as significant.

In the regularized Stokes formulation, the computation of the sums in Eqs. (32) and (33) represents an M -body problem, where each immersed boundary point contributes to the velocity of every point. This is the most time-consuming part of the method. Although there are fast summation techniques, such as the fast multipole method, that may be used to speed up this part of the computation, even using a simple OpenMP parallelization of the velocity calculation with 2 processors is enough to speed up the computation by a factor of 1.74 compared to the serial computation (see Table 3). Using 4 processors for the velocity computation, the program ran 2.7 times faster than the serial case. The table also shows the memory usage of the two methods. The required memory in the regularized Stokes formulation increases only slightly when more processors are used. However, the amount of memory required is significantly smaller than that of the gIB method, which has to store variables on a three-dimensional grid.

In applications of swimming flagella, where the dynamics of the elastic rod may be driven by a time dependent strain twist vector, the outcome of interest may be the swimming speed or trajectory of the flagella. These applications typically require long-time simulations, so that the speed-up obtained with the regularized Stokes formulation compared to the gIB method can have a considerable impact. Overall, the regularized Stokes formulation has a substantial decreased computation time and a decreased memory usage in comparison to the gIB method.

6.4. Motion of an undulatory flagellum

This regularized Stokes formulation of an elastic rod can be used to investigate the hydrodynamics of eukaryotic flagella that use an undulatory motion to propel themselves forward [43,36]. Eukaryotic flagella have a distinct structure composed of 9 sets of microtubule doublets in a circular structure surrounding a central pair of microtubule doublets. For example, in sperm, there are dynein motors (active force generators) along the length of the microtubules that cause the microtubule doublets to slide relative to one another, generating the propagation of a flagellar bending wave [44,45]. (This is in contrast to prokaryotic flagella, such as *Escherichia coli*, that have a different internal structure where movement is generated by a rotary motor at the base of the flagellum.) Flagella are thin and flexible, with length much greater than radius, therefore we can idealize them as an elastic rod. Since most flagella are on the length scale of microns, flagellar motility is in the regime where viscous forces dominate [43,46] and we can describe the fluid with the Stokes equations.

We model a single flagellum as a filament or rod in three spatial dimensions, keeping track of the centerline and the orthonormal triads. In this framework, we model the undulatory motion using a preferred curvature function that corresponds to a sine wave with a prescribed frequency and amplitude. In this initial study, we explore the validity of this algorithm to model a planar undulatory motion, i.e., a flagellum with lateral displacement (in the y plane), that propagates along the length of the flagellum (in the z plane). Specifically, as detailed in Section 2, the intrinsic curvature of the flagellum is given as $\kappa = \sqrt{\Omega_1^2 + \Omega_2^2}$. To create planar motion of the flagellum, we set $\Omega_2 = \Omega_3 = 0$ and model a wave of lateral displacement along the length of the rod by choosing Ω_1 as:

$$\Omega_1(s, t) = -k^2 b \sin(ks + \sigma t), \quad (50)$$

corresponding to a sine wave with $z(s, t) = s$ and $y(s, t) = b \sin(ks + \sigma t)$ (up to translations and rotations), where the undulating flagellum has wavelength $2\pi/k$, amplitude b , frequency σ , and s is the material parameter along the centerline of the flagellum. (Since the propagating wave is planar, we have $x(s, t) = 0$ for all time.) In contrast to the open and closed rod examples presented earlier, Ω_1 given in Eq. (50) is a function of space and time. All parameters used for these simulations are detailed in Table 4.

In a seminal paper by Taylor [47], a mathematical analysis was completed for a waving, infinite cylinder in a Newtonian fluid. The classical asymptotic results of this paper approximate the swimming speed V of the infinite cylinder to first order as

Table 3
Computational time (RegSto stands for regularized Stokes formulation).

| Method | Numerical case | Wall time (hour:min:sec) | Mem (kb) |
|------------------|----------------|--------------------------|----------|
| gIB (serial) | Closed rod | 15:12:27 | 87532 |
| RegSto (serial) | Closed rod | 1:15:14 | 4808 |
| RegSto (2 nodes) | Closed rod | 0:43:16 | 4880 |
| RegSto (4 nodes) | Closed rod | 0:27:57 | 5020 |

Table 4
Computational parameters for numerical study of undulatory flagellum.

| Parameter | Value |
|--|--|
| Unstressed rod length, L | 40 μm |
| Immersed Boundary points, M | 600 |
| Meshwidth for rod, Δs | 0.0667 μm |
| Time step, Δt | 1×10^{-6} s |
| Fluid viscosity, μ | 1×10^{-6} g μm^{-1} s $^{-1}$ |
| Regularization parameter, ε | 7 Δs μm |
| Bending modulus ($a_1 = a_2$) | 3.5×10^{-2} g μm^3 s $^{-2}$ |
| Twist modulus (a_3) | 3.5×10^{-2} g μm^3 s $^{-2}$ |
| Shear modulus ($b_1 = b_2$) | 8.0×10^{-1} g μm^3 s $^{-2}$ |
| Stretch modulus (b_3) | 8.0×10^{-1} g μm^3 s $^{-2}$ |
| Frequency of undulation, σ | Varied 250–550 Hz |
| Amplitude of undulation, b | Varied 0.075–1.5 μm |
| Wavelength of undulation, $2\pi/k$ | wavelength = 5 μm ($k = 2\pi/5 \mu\text{m}^{-1}$) |
| Curvature in direction of \mathbf{D}^1, Ω_1 | $-k^2 b \sin(ks + \sigma t) \mu\text{m}^{-1}$ |
| Curvature in direction of \mathbf{D}^2, Ω_2 | 0 μm^{-1} |
| Intrinsic twist, Ω_3 | 0 μm^{-1} |

$$V = \frac{1}{2} k \sigma b^2 \left(\frac{K_o(kr_c) - \frac{1}{2}}{K_o(kr_c) + \frac{1}{2}} \right), \tag{51}$$

valid for $kr_c \ll 1$, where b is the amplitude, σ is the frequency, $\lambda = 2\pi/k$ is the wavelength, r_c is the radius of the cylindrical tube, and K_o is the zeroth order modified Bessel equation of the second kind.

Simulations of the model were run using the parameters in Table 4 in order to compare swimming speeds of the regularized Stokes formulation of an elastic rod, where the intrinsic curvature is specified as a small amplitude sinusoidal wave of displacement. The simulations were performed on a finite elastic rod that is 8 wavelengths long in order to minimize end-point effects. In order to compare the swimming speed from the simulations and the first order swimming speed of Taylor in Eq. (51), the parameter r_c needs to be specified. In the model of the elastic rod, we do not specify the radius of the rod. However, in specifying a cutoff function as in Eq. (12) and a regularization parameter $\varepsilon = 7\Delta s$, most of the force and torque is being applied within a radius of $7\Delta s$. Since the cutoff function has infinite support, the regularization parameter is a rough estimate of the approximate radius. Therefore, we choose to set $r_c = 10\Delta s$ to compare to the results of Taylor.

In Fig. 6(a) and (b), the swimming velocities using the regularized Stokes formulation are shown with markers of varying types. Note that in Fig. 6(a), as the amplitude b increases for a given fixed frequency, the swimming speed is increasing quadratically, as expected from Taylor’s results given in Eq. (51). Similarly, in Fig. 6(b), as the frequency σ of the undulation increases for a fixed amplitude, the swimming speed increases linearly. In both Fig. 6(a) and (b), we have also plotted dashed curves, which are for the Taylor approximation of the swimming speed as calculated from Eq. (51). The swimming speeds in Fig. 6(a) have better agreement between Taylor’s analysis and the simulations for smaller amplitudes. There is also better agreement between Taylor’s analysis and the results of the computational model for lower frequencies in Fig. 6(b). Note also that simulation results did not match as well for shorter length rods (results not shown for rods of 10 μm , and 20 μm). Overall, the comparison between theory and simulations have good agreement. We emphasize here that Taylor’s first order

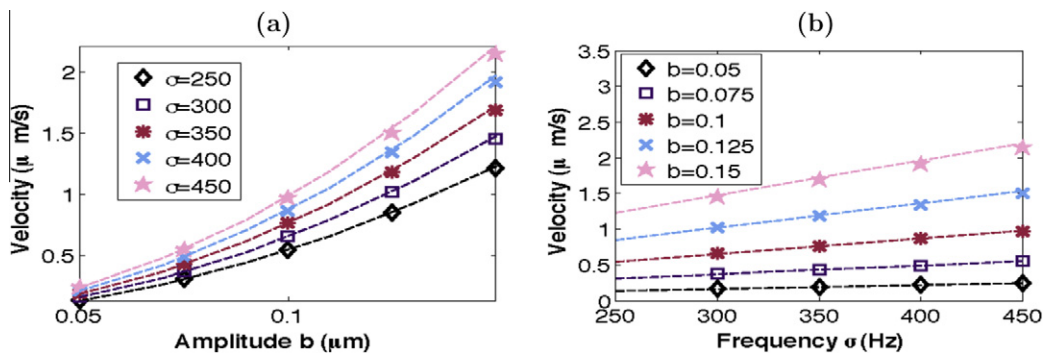


Fig. 6. Swimming speed of flagellum, where amplitude and frequency of the undulation are specified in terms of a wave of lateral displacement. In (a), swimming speed is shown as a function of amplitude for varying frequencies and in (b), swimming speed is shown as a function of frequency for varying amplitude. The markers are from simulations and the dashed lines correspond to swimming speed calculated from Taylor’s analysis, given in Eq. (51) [47].

approximation of swimming speed is valid for $kr_c \ll 1$ and for an infinite cylinder, whereas the flagellum in our simulations has finite length with a propagating sine wave.

7. Discussion and conclusions

In this paper, we have derived and implemented a regularized Stokes formulation that describes an elastic rod with intrinsic curvature and twist that is immersed in a viscous, incompressible fluid. The elasticity of the rod is governed by a Kirchhoff rod model in which the rod is described by a space curve corresponding to the centerline and an associated orthonormal triad to capture the bend and twist of the rod. This formulation extends the method of regularized Stokeslets, capturing the twist of the rod. In this formulation, the rod now applies both force and torque to the surrounding fluid, and the rod moves according to the linear velocity and rotates according to the angular velocity. The solution of the linear and angular velocity is determined as a superposition of fundamental solutions: Stokeslets, rotlets, and dipoles.

We motivate the development of this method as a way to model zero Reynolds number applications with a decreased computation time. The open and closed rods presented in Sections 6.1 and 6.2, are numerical examples of rods or filaments at the microscale that are immersed in a fluid. In these examples, we verify that results of this model matched well with results of elastic rod theory. Additionally, results for equilibrium configurations and energy profiles were the same as those from the gIB method which considers the full Navier–Stokes equations. The computational efficiency of this algorithm is shown in Section 6.3; the regularized Stokes formulation is 12 times faster than the gIB method and uses less memory. The speed up in computation time is attributed to using regularized fundamental solutions to calculate the velocities and to the use of one curvilinear mesh for the rod. This is in contrast to the gIB method that uses a Cartesian grid for the fluid variables and a curvilinear mesh for the rod.

This regularized Stokes formulation of an elastic rod with intrinsic curvature and twist has many low Reynolds number applications. Examples include modeling DNA supercoiling and motility of microorganisms that are propelled by a flagellum, where these structures can be idealized as elastic rods. As a proof of concept, in Section 6.4, we used the regularized Stokes formulation derived in this paper to model an undulatory filament. A time dependent intrinsic curvature is assigned that corresponded to waves of lateral displacement along the length of the rod. The utility of this application is verified by good agreement of the swimming speeds computed from the simulations in comparison to the classical results of Taylor for an infinite cylinder [47].

This algorithm has been derived, implemented, and verified through several numerical examples. There are still a number of open questions and analyses to be completed in the future. Further investigation will be completed to determine how this regularized Stokes formulation can be extended and used to study applications of elastic rods with self-contact. One avenue of future research involves studying the regularization parameter ε . This parameter does not correspond directly to the radius of the rod and it does affect the solution, as shown in Figs. 2 and 4. Future work will study an optimal value of ε , which will most likely be problem dependent. In the same area, future research will also investigate the choice of blob function on the results. Additionally, a complete error analysis of this regularized Stokes formulation remains to be completed for the regularization and discretization error.

Acknowledgements

The work of S. Olson was supported, in part, by NSF DMS 1122461. S. Lim acknowledges support, in part, by NSF DMS 0815751. The authors thank L. Fauci for helpful discussions.

Appendix A

We derive complete forms of the linear velocity and angular velocity at any point used in this paper as a fundamental solution of the regularized Stokes equations:

$$\mathbf{0} = -\nabla p + \mu \Delta \mathbf{u} + \mathbf{f}_o \psi_\varepsilon + \frac{1}{2} \nabla \times \mathbf{n}_o \psi_\varepsilon, \quad (52)$$

$$\mathbf{0} = \nabla \cdot \mathbf{u}. \quad (53)$$

First, we derive the linear velocity. Given that ψ_ε is the cutoff function, let G_ε and B_ε be the regularized Green's function and biharmonic function, respectively, satisfying the following equations:

$$\Delta G_\varepsilon = \psi_\varepsilon \quad \text{and} \quad \Delta B_\varepsilon = G_\varepsilon, \quad (54)$$

where ψ_ε , G_ε and B_ε are functions of r , where $r = \|\mathbf{x} - \mathbf{X}_o\|$ and ε is a parameter that controls the spreading size of the blob function. Taking the divergence of Eq. (52), we can simplify it as follows:

$$\begin{aligned} \nabla \cdot \nabla p &= \mu \nabla \cdot (\Delta \mathbf{u}) + \nabla \cdot \left(\mathbf{f}_o \psi_\varepsilon + \frac{1}{2} \nabla \times \mathbf{n}_o \psi_\varepsilon \right) = \mu \nabla \cdot (\Delta \mathbf{u}) + \nabla \cdot (\mathbf{f}_o \psi_\varepsilon) + \frac{1}{2} \nabla \cdot (\nabla \times \mathbf{n}_o \psi_\varepsilon) \\ &= 0 + \psi_\varepsilon \nabla \cdot \mathbf{f}_o + \mathbf{f}_o \cdot \nabla \psi_\varepsilon + 0 = \mathbf{f}_o \cdot \nabla \psi_\varepsilon. \end{aligned} \tag{55}$$

Here we have used the fact that the fluid is incompressible, \mathbf{f}_o is a constant vector, and $\nabla \cdot (\nabla \times \mathbf{A}) = \mathbf{0}$ for any vector field \mathbf{A} . We now solve for the fluid pressure, p :

$$\Delta p = \mathbf{f}_o \cdot \nabla \psi_\varepsilon = (\mathbf{f}_o \cdot \nabla) \Delta G_\varepsilon = \Delta (\mathbf{f}_o \cdot \nabla G_\varepsilon) \tag{56a}$$

$$\Rightarrow p = \mathbf{f}_o \cdot \nabla G_\varepsilon \tag{56b}$$

By substituting a particular solution for the pressure in Eq. (56b) into Eq. (52), we solve for the fluid velocity:

$$\begin{aligned} \mu \Delta \mathbf{u} &= \nabla p - \mathbf{f}_o \psi_\varepsilon - \frac{1}{2} \nabla \times \mathbf{n}_o \psi_\varepsilon \\ &= \nabla (\mathbf{f}_o \cdot \nabla G_\varepsilon) - \mathbf{f}_o \psi_\varepsilon - \frac{1}{2} \nabla \times \mathbf{n}_o \psi_\varepsilon \\ &= \nabla (\mathbf{f}_o \cdot \nabla (\Delta B_\varepsilon)) - \mathbf{f}_o \Delta G_\varepsilon - \frac{1}{2} \nabla \psi_\varepsilon \times \mathbf{n}_o \\ &= (\mathbf{f}_o \cdot \nabla) \nabla (\Delta B_\varepsilon) - \mathbf{f}_o \Delta G_\varepsilon - \frac{1}{2} \nabla (\Delta G_\varepsilon) \times \mathbf{n}_o. \end{aligned} \tag{57}$$

Then the solutions of the regularized Stokes equations for given point forces and torques are as follows,

$$\mu \mathbf{u}(\mathbf{x}) = (\mathbf{f}_o \cdot \nabla) \nabla B_\varepsilon(\mathbf{x} - \mathbf{X}_o) - \mathbf{f}_o G_\varepsilon(\mathbf{x} - \mathbf{X}_o) + \frac{1}{2} \mathbf{n}_o \times \nabla G_\varepsilon(\mathbf{x} - \mathbf{X}_o), \tag{58}$$

$$p(\mathbf{x}) = \mathbf{f}_o \cdot \nabla G_\varepsilon(\mathbf{x} - \mathbf{X}_o), \tag{59}$$

for any $\mathbf{x} \in \mathbb{R}^3$. Therefore, Eqs. (58) and (59) can be used to evaluate the motion of the centerline of the rod as well as at any point in the surrounding fluid.

Second, we evaluate the angular velocity from Eq. (58) as follows:

$$\begin{aligned} \mu \boldsymbol{\omega} &= \frac{1}{2} \nabla \times (\mu \mathbf{u}) \\ &= \frac{1}{2} \nabla \times [(\mathbf{f}_o \cdot \nabla) \nabla B_\varepsilon] - \frac{1}{2} \nabla \times [\mathbf{f}_o G_\varepsilon] - \frac{1}{4} \nabla \times (\nabla \times (\mathbf{n}_o G_\varepsilon)) \\ &= 0 + \frac{1}{2} (\mathbf{f}_o \times \nabla G_\varepsilon) + \frac{1}{4} \mathbf{n}_o \Delta G_\varepsilon - \frac{1}{4} \nabla (\mathbf{n}_o \cdot \nabla G_\varepsilon) \\ &= \frac{1}{2} (\mathbf{f}_o \times \nabla G_\varepsilon) + \frac{1}{4} \mathbf{n}_o \psi_\varepsilon - \frac{1}{4} (\mathbf{n}_o \cdot \nabla) \nabla G_\varepsilon. \end{aligned} \tag{60}$$

Here we have used the vector identities that $\nabla \times (\nabla g) = \mathbf{0}$ for any scalar function g and $\nabla \times (\nabla \times \mathbf{A}) = \nabla(\nabla \cdot \mathbf{A}) - \nabla^2 \mathbf{A}$ for any vector field \mathbf{A} .

As an example, we make a particular choice of the cutoff function ψ_ε given by

$$\psi_\varepsilon(r) = \frac{15\varepsilon^4}{8\pi(r^2 + \varepsilon^2)^{7/2}},$$

which satisfies

$$4\pi \int_0^\infty r^2 \psi_\varepsilon(r) dr = 1.$$

Then G_ε is given as

$$G_\varepsilon(r) = -\frac{3\varepsilon^2 + 2r^2}{8\pi(\varepsilon^2 + r^2)^{3/2}},$$

where

$$\begin{aligned} G'_\varepsilon(r) &= \frac{2r^3 + 5r\varepsilon^2}{8\pi(\varepsilon^2 + r^2)^{5/2}}, & B'_\varepsilon(r) &= -\frac{r}{8\pi(\varepsilon^2 + r^2)^{1/2}}, \\ G''_\varepsilon(r) &= \frac{5\varepsilon^4 - 14r^2\varepsilon^2 - 4r^4}{8\pi(\varepsilon^2 + r^2)^{7/2}}, & B''_\varepsilon(r) &= -\frac{\varepsilon^2}{8\pi(\varepsilon^2 + r^2)^{3/2}}. \end{aligned}$$

The explicit form of the linear velocity and the fluid pressure are as follows:

$$\mu \mathbf{u}(\mathbf{x}) = \mathbf{f}_o H_1(r) + [\mathbf{f}_o \cdot (\mathbf{x} - \mathbf{X}_o)](\mathbf{x} - \mathbf{X}_o) H_2(r) + \frac{1}{2} [\mathbf{n}_o \times (\mathbf{x} - \mathbf{X}_o)] Q(r), \quad (61)$$

$$p(\mathbf{x}) = [\mathbf{f}_o \cdot (\mathbf{x} - \mathbf{X}_o)] Q(r), \quad (62)$$

where

$$H_1(r) = \frac{B'_\varepsilon(r)}{r} - G_\varepsilon(r) = \frac{2\varepsilon^2 + r^2}{8\pi(\varepsilon^2 + r^2)^{3/2}}, \quad (63)$$

$$H_2(r) = \frac{rB''_\varepsilon(r) - B'_\varepsilon(r)}{r^3} = \frac{1}{8\pi(r^2 + \varepsilon^2)^{3/2}}, \quad (64)$$

$$Q(r) = \frac{G'_\varepsilon(r)}{r} = \frac{5\varepsilon^2 + 2r^2}{8\pi(\varepsilon^2 + r^2)^{5/2}}, \quad (65)$$

and the explicit form of the angular velocity is given as

$$\mu \mathbf{w}(\mathbf{x}) = \frac{1}{2} [\mathbf{f}_o \times (\mathbf{x} - \mathbf{X}_o)] Q(r) + \frac{1}{4} \mathbf{n}_o D_1(r) + \frac{1}{4} (\mathbf{n}_o \cdot (\mathbf{x} - \mathbf{X}_o)) (\mathbf{x} - \mathbf{X}_o) D_2(r), \quad (66)$$

where

$$D_1(r) = \psi_\varepsilon(r) - \frac{G'_\varepsilon(r)}{r} = \frac{10\varepsilon^4 - 7\varepsilon^2 r^2 - 2r^4}{8\pi(\varepsilon^2 + r^2)^{7/2}}, \quad (67)$$

$$D_2(r) = \frac{G'_\varepsilon(r)}{r^3} - \frac{G''_\varepsilon(r)}{r^2} = \frac{21\varepsilon^2 + 6r^2}{8\pi(\varepsilon^2 + r^2)^{7/2}}, \quad (68)$$

and $Q(r)$ is the same as in Eq. (65).

References

- [1] E. Dill, Kirchhoff's theory of rods, Arch. Hist. Exact. Sci. 44 (1992) 1–23.
- [2] C. Benham, Onset of writhing in circular elastic polymers, Phys. Rev. A 35 (1989) 2582–2586.
- [3] A. Goriely, M. Tabor, The nonlinear dynamics of filaments, Nonlinear Dyn. 21 (2000) 101–133.
- [4] N. Chouaieb, A. Goriely, M. JH, Helices, Proc. Natl. Acad. Sci. USA 103 (2006) 9398–9403.
- [5] I. Klapper, Biological applications of the dynamics of twisted elastic rods, J. Comput. Phys. 125 (1996) 325–337.
- [6] E. Zajac, Stability of two planar loop elasticas, J. Appl. Mech. 29 (1962) 136–142.
- [7] T. Bishop, R. Cortez, O. Zhmudsky, Investigation of bend and shear waves in a geometrically exact elastic rod model, J. Comput. Phys. (2004) 642–665.
- [8] B. Coleman, D. Swigon, Theory of supercoiled configurations with self-contact and its application to DNA plasmids, J. Elasticity 60 (2000) 173–221.
- [9] B. Coleman, D. Swigon, I. Tobias, Elastic stability of DNA configurations. II. Supercoiled plasmids with self contact, Phys. Rev. E 61 (2000) 2–23.
- [10] B. Coleman, D. Swigon, Theory of self-contact in kirchhoff rods with applications to supercoiling of knotted and unknotted DNA plasmids, Philos. Trans. R. Soc. Lond. Ser. A: Math. Phys. Eng. Sci. 362 (2004) 1281–1299.
- [11] A. Goriely, M. Tabor, Nonlinear dynamics of filaments I. Dynamical instabilities, Phys. D 105 (1997) 20–44.
- [12] A. Goriely, M. Tabor, Nonlinear dynamics of filaments II. Nonlinear analysis, Phys. D 105 (1997) 45–61.
- [13] R. Goldstein, T. Powers, C. Wiggins, Viscous nonlinear dynamics of twist and writhe, Phys. Rev. Lett. 80 (1998) 5232–5235.
- [14] C. Wolgemuth, R. Goldstein, T. Powers, Dynamic supercoiling bifurcations of growing elastic filaments, Phys. D (2004) 266–289.
- [15] B. Griffith, S. Lim, Simulating an elastic ring with bend and twist by an adaptive generalized immersed boundary method, Commun. Comput. Phys. 12 (2012) 433–461.
- [16] S. Lim, A. Ferent, X. Wang, C. Peskin, Dynamics of a closed rod with twist and bend in fluid, SIAM J. Sci. Comput. 31 (2008) 273–302.
- [17] S. Lim, Dynamics of an open elastic rod with intrinsic curvature and twist in a viscous fluid, Phys. Fluids 22 (2010) 024104–1–024104–11.
- [18] T. Schlick, Modeling superhelical DNA: recent analytical and dynamic approaches, Curr. Opin. Struct. Biol. 5 (1995) 245–262.
- [19] T. Schlick, W. Olson, Trefoil knotting revealed by molecular dynamics simulations of supercoiled DNA, Science 257 (1992) 266–289.
- [20] T. Strick, J. Allemand, D. Bensimon, V. Croquette, Behavior of supercoiled DNA, Biophys. J. 74 (1998) 2016–2028.
- [21] R. Vogel, H. Stark, Force-extension curves of bacterial flagella, Eur. Phys. J. E 33 (2010) 259–271.
- [22] N. Mendelson, Helical growth of *Bacillus subtilis*: a new model of cell growth, Proc. Natl. Acad. Sci. USA 73 (1976) 1740–1744.
- [23] N. Mendelson, Bacterial growth and division: genes, structures, forces, and clocks, Microbiol. Rev. 46 (1982) 341–375.
- [24] N. Mendelson, J. Thwaites, J. Kessler, C. Li, Mechanics of bacterial macrofiber initiation, J. Bacteriol. (1995) 7060–7069.
- [25] L. Greengard, M. Kropinski, Integral equation methods for Stokes flow in doubly-periodic domains, J. Eng. Math 48 (2004) 150–170.
- [26] X. Wang, J. Kanapka, W. Ye, N. Aluru, J. White, Algorithms in FastStokes and its application to micromachined device simulation, J. Eng. Math. 25 (2006) 248–257.
- [27] X. Wang, T. Lei, J. Huang, Z. Yao, A parallel fast multipole accelerated integral equation scheme for 3D Stokes equations, Int. J. Numer Methods Eng. 70 (2007) 248–257.
- [28] J. Lighthill, Flagellar hydrodynamics, SIAM Rev. 18 (1976) 161–230.
- [29] J. Keller, S. Rubinow, Slender-body theory for slow viscous flow, J. Fluid Mech. 75 (1976) 705.
- [30] M. Shelley, T. Ueda, The Stokesian hydrodynamics of flexing, stretching filaments, Physica D 14 (2000) 221.
- [31] T. Bringley, S. Peskin, Validation of a simple method for representing spheres and slender bodies in an immersed boundary method for Stokes flow on an unbounded domain, J. Comput. Phys. 227 (2008) 5397–5425.
- [32] R. Cortez, The method of regularized Stokeslets, SIAM J. Sci. Comput. 23 (2001) 1204–1225.
- [33] R. Cortez, L. Fauci, A. Medovikov, The method of regularized Stokeslets in three dimensions: analysis, validation, and application to helical swimming, Phys. Fluids 17 (2005) 0315041–03150414.
- [34] B. Cummins, T. Gedeon, I. Klapper, R. Cortez, Interaction between arthropod filiform hairs in a fluid environment, J. Theor. Biol. (2007) 266–280.

- [35] H. Flores, E. Lobaton, S. Mendez-Diez, S. Tlupova, R. Cortez, A study of bacterial flagellar bundling, *Bull. Math Biophys.* 65 (2005) 137–168.
- [36] E. Gillies, R. Cannon, R. Green, A. Pacey, Hydrodynamic propulsion of human sperm, *J. Fluid Mech.* 625 (2009) 445–474.
- [37] S. Olson, S. Suarez, L. Fauci, Coupling biochemistry and hydrodynamics captures hyperactivated sperm motility in a simple flagellar model, *J. Theor. Biol.* 283 (2011) 203–216.
- [38] A. Tornberg, M. Shelley, Simulating the dynamics and interactions of flexible fibers in stokes flows, *J. Comp. Phys.* 196 (2004) 8–40.
- [39] S. Lim, C. Peskin, Fluid–mechanical interaction of flexible bacterial flagella by the immersed boundary method, *Phys. Rev. E* 85 (2012) 036307.
- [40] S. Goyal, N. Perkins, C. Lee, Nonlinear dynamics and loop formation in kirchhoff rods with implications to the mechanics of DNA and cables, *J. Comput. Phys.* 279 (2005) 371.
- [41] A. Love, *A Treatise on the Mathematical Theory of Elasticity*, 4th ed., Cambridge Univ. Press, Dover, New York, 1927.
- [42] L. Landua, E. Lifschitz, *Theory of elasticity*, 3rd ed., Pergamon, Oxford, 1986.
- [43] L. Fauci, R. Dillon, Biofluidmechanics of reproduction, *Annu. Rev. Fluid Mech.* 38 (2006) 371–394.
- [44] G. Vernon, D. Woolley, Basal sliding and the mechanics of oscillation in a mammalian sperm flagellum, *Biophys. J.* 87 (2004) 3934–3944.
- [45] D. Woolley, Flagellar oscillation: a commentary on proposed mechanisms, *Biol. Rev.* 85 (2010) 453–470.
- [46] E. Gaffney, H. Gadelha, D. Smith, J. Blake, J. Kirkman-Brown, Mammalian sperm motility: observation and theory, *Annu. Rev. Fluid Mech.* 43 (2001) 501–528.
- [47] G. Taylor, The action of waving cylindrical tails in propelling microscopic organisms, *Proc. R. Soc. Lond. Ser. A* 211 (1952) 225–239.